Very long Wavelength Intersubband Infrared Hot Electron Transistor

Sarath D. Gunapala, John K. Liu, True L, Lin, and Jin S. Park

Center for Space Microelectronics Technology
Jet Propulsion Laboratory, California Institute of Technology
Pasadena, CA 91109, U.S.A.

ABSTRACT

We have demonstrated the first very long wavelength (16 μm) infrared hot electron transistor (IHET). This device utilizes a bound to continuum GaAs/$Al_xGa_{1-x}As$ (x==O.11) quantum well infrared photodetector (QWIP) as a photosensitive emitter, a wide quantum well as a base, and a thick $Al_xGa_{1-x}As$ (x=0. 11) barrier between the base and the collector as an energy discriminating filter. This energy filter blocks the lower energy electrons, which drain through the base while higher energy photo electrons pass to the collector. Therefore, the defectivity of the device at the collector is much higher than the defectivity at the emitter.

KEYWORDS: quantum well, hot electron, intersubband, infrared detectors and long wavelength

1. INTRODUCTION

Very long wavelength infrared (IR) detectors and imaging systems are required in many space applications such as the Atmospheric IR Sounder (AIRS) and the Tropospheric Emission Spectrometer (TES) instruments which will be used in NASA's Earth Observation System (EOS). The wavelength of the IR radiation required in these applications range from 3.7 to 15.4μm. These space applications have placed stringent requirements on the performance of the IR detectors and arrays including high defectivity, low dark current, uniformity and radiation hardness. This paper will present the study and development of a low dark current very long wavelength intersubband IR hot electron transistor (IHET).

There has been a lot of interest recently in the detection of very long wavelength (λ = 12-16 μm) infrared radiation using multiple quantum wells, due to the fact that these quantum well IR photodetectors [1-13] (QWIPs) and IHET's [8,14-16] can be fabricated using the mature III-V materials growth and processing technologies. This superior materials control results in high uniformity and thus allows fabrication of large staring arrays (1= 8-12 pm) with excellent imaging performance [17-19]. One of the problems associated with the very long wavelength QWIPs is the higher dark current which adversely affects detector performance. By analyzing the dark current of shallow quantum wells we have realized that the total tunneling current (sequential tunneling + thermionic assisted tunneling) is significantly higher than the thermionic dark current (Fig. 1). The conduction electrons carrying these two tunneling current components are lower in energy than the photoelectrons [8]. Therefore, a 16μm $GaAs/Al_xGa_{1-x}As$ IHET which can effectively filter out sequential tunneling and thermionic assisted tunneling currents was fabricated.

2. DARK CURRENT

In this section the dark current of a single quantum well, which has intersubband absorption peak at 16 μm will be analyzed. First effective number of electrons [11,20] n(V) which are thermally excited into the continuum transport states, as a function of bias voltage V were calculated.

$$n(v) = \left(\frac{m^*}{\pi\hbar^2 L_p}\right)\int_{E_0}^{\infty} f(E)T(E,V)dE$$

The first factor containing the effective mass m* represents the average three dimensional density of states. Where L_p is the superlattice period, f(E) is the fermi factor $f(E) = [1+\exp(E-E_0-E_F)/KT]^{-1}$, E_0 is the bound state energy, E_F is the two-dimensions] fermi energy, E is the energy of the electron, and T(E,V) is the tunneling current transmission factor. This tunneling transmission factor obtained by applying WKB approximation to a biased quantum well is:

$$T(E) = (4\sqrt{E}\sqrt{(V_0 - E)} / V_0)e^{-2\tau}$$

where $\tau = (2L\sqrt{2m^*} / 3\hbar\Delta V)(V_0 - E)^{\frac{3}{2}}$, V. is the barrier height, AV is the bias voltage pcr superlattice period, and L is the barrier width. The number of electrons,

given by n(V) accounts for thermionic emission above the barrier height when $E>V_0$ and thermionic assisted tunneling and tunneling when $E<V_0$. Then the bias-dependent dark current $I_d(V)$ was calculated, using $I_d(V) = eAn(V)v(V)$, where v(V) is the average transport velocity , A is the device area, and e is the electronic charge. The average transport velocity was calculated using $v(V) = \mu F[1+(\mu F/v_s)^2]^{-1/2}$, where μ is the mobility, F is the electric field, and v_s is the saturated drift velocity. In order to obtain T = 60K bias-dependent dark current $\mu = 1200$ cm²/V s, and $v_s = 5.5\times10^6$ cm/s was used. Fig. 1 shows the T= 60K dark current due to thermionic emission, total dark current (thermionic + thermionic assisted tunneling + tunneling), and experimental dark current of a QWIP sample which has wavelength cutoff $\lambda_c = 17.8$ pm. According to the calculations tunneling through the barriers dominate the dark current at temperatures below 30K, at temperatures between 40-60K thermionic assisted tunneling might become important, and at temperatures above 60K thermionic emission into the continuum transport states dominate the dark current.

3. EXPERIMENT

As shown in Fig. 2 the device structure consisted of a multi-quantum well region of 50 periods of 500 Å undoped $Al_{0.11}Ga_{0.89}As$ barrier and 65 Å doped GaAs well. The quantum wells were doped to n = 5x1017 cm^{-3}, and sandwiched between a heavily doped (n = 1x1018 cm^{-3}) 1 µm GaAs contact layer at the bottom as the emitter contact and a doped (n = 3×10^{17} cm^{-3}) 500 Å GaAs layer on the top as the base contact. On top of the base a 2000 Å undoped $Al_{0.11}Ga_{0.89}As$ layer and a doped (n = 3×10^{17} cm-$ 0.5 µm GaAs layer were grown. The 2000 Å undoped $Al_{0.11}Ga_{0.89}As$ As layer acted as a discriminator between the tunnel-electrons and photo-electrons, and the top 0.5 µm GaAs layer served as the collector. This device structure was grown on a semi-insulating GaAs substrate using molecular beam epitaxy.

The intersubband absorption was measured on a 45" polished multipass waveguide 2[1]) as shown in the inset of Fig. 3. As shown in the Fig. 3 the T = 300K absorption coefficient spectra α_p has a peak infrared absorption coefficient $\alpha_p = 534$ cm^{-1} at $\lambda_p = 17{,}1$ µm with absorption half heights at 14.2 and 18 µm (i.e., a full width at half maximum of $\Delta\lambda = 3.8$ pm). At low temperature the half width narrows and the peak absorption coefficient increases [22,23]) by a factor of 1.3 so that $\alpha_p = 694$ cm^{-1} at T = 60K corresponding to an unpolarized quantum efficiency $\eta = (1 - e^{-2\alpha\ell})/2 = 16.5\%$.

To facilitate the application of bias to the quantum well structure, the following processing steps were carried out. First arrays of 200x200 µm² square collectors were chemically etched. in the next processing step the 6.25x 10-4 cm² QWIP mesas which overlap with collector mesas were etched. Finally, Au/Ge ohmic contacts were evaporated onto the emitter, base and collector contact layers. The emitter and collector dark currents versus base-collector bias voltage are shown in Fig. 4. "l'his figure also shows the lower energy dark current filtration capability of the quantum filter. The dark current transfer ratio$\left(\alpha_d = I_{C(dark)}/I_{E(dark)}\right)$ is 7.2×10^{-5} at operating base-collector bias voltage $V_{CB} = -42$ mV.

These 200x200 µm² square detectors were back illuminated through a 45" polished facet as described in detail previously [1]) and responsivity spectra were measured

with a tunable source consisting of a 1OOOK blackbody and a grating monochromator. The emitter and collector responsivity spectrum measured at 7 = 60K is shown in Fig. 5. The values of the peak wavelength λ_p, cutoff wavelength λ_c and the spectral width ($\Delta\lambda$ /Z) (full width at half maximum) are 16.3 μm, 17.3 μm and 20% respectively. The absolute responsivity was measured by two different methods, comparison with calibrated pyroelectric detector and, using a calibrated blackbody source. The peak responsivity Rp of the detector was 400 mA/W, while the peak responsivity and the shape of the spectra were independent of the measuring technique as expected. Fig. 6 shows the IHET emitter and collector photo currents versus base-collector voltage at T = 60K. The emitter was kept at -1 V bias relative to the base potential, Due to the hot electron relaxation in the wide base region, the photo current at collector is smaller relative to the emitter photo current. Photo current transfer ratio ($\alpha_p = I_{C(photo)} / I_{E(photo)}$) is 1.2x10-1 at V_{CB} = -42 mV. It is worth noticing that α_d is more than three orders of magnitude smaller than α_p.

4. RESULTS

The optical gain g of the detector determined from R = (e/ hν)ηg is given by g = 0.2. The noise current [24]) i_n was calculated using $i_n = \sqrt{4eI_d g\Delta f}$, where Af is the bandwidth. The calculated noise current of the detector is i_n = 17 pA at T = 60K. The peak D* can now be calculated from D* = R $\sqrt{A\Delta f}$ /i_n. The calculated D* between the emitter and the base (QWIP) at V_{EB} = -IV, V_{CB} = -42 mV and T = 60K is 5.8×10^8 cm√Hz/W. The defectivity D* at the collector (IHET) is determined) from D^*(IHET) = $(\alpha_p/\sqrt{\alpha_d})\,D^*$(QWIP) is given by D^*(IHET) = 8.2x109 cm√Hz/W at 'I" = 60K. As shown in Fig. 7 defectivity D^* increases dramatically with decreasing temperature reaching D* = 1×10^{12} cm√Hz/W at T = 25 K and is even larger at lower temperatures. In contrast, detectivit y D^* of HgCdTe detectors are saturated as the temperature is lowered.

S. CONCLUSION

In conclusion, we have demonstrated the first very long wavelength (kc = 17.3 pm) IHET. This device clearly shows the dark current filtration capability of the energy filter. Therefore, the D* of IHET is much higher than the D* of two terminal multi quantum well detector.

ACKNOWLEDGMENTS

We are grateful to K. K. Choi of the Army Research Laboratory and K. M. S. V. Bandara and B. F. Levine of the AT&T Bell Laboratories for many useful discussions and C. A. Kukkonen, V. Sarohia, S. Khanna, K. M. Koliwad, B. A. Wilson, and P. J. Grunthaner of the Jet Propulsion Laboratory for encouragement and support of this work. The research described in this paper was performed by the Center for space Microelectronics Technology, Jet Propulsion Laboratory, California Institute of Technology, and was jointly sponsored by the Ballistic Missile Defense Organization/Innovative Science and Technology Office, and the National Aeronautics and Space Administration, Office of Advanced Concepts and Technology.

REFERENCES

1) B. F. Levine, C. G. Bethea, G. Hasnain, J. Walker, and R. J. Malik, Appl. Phys. Lett. S3-(1988) 2.96.

2) B. F. Levine, *Proceedings of the NATO Advanced Research Workshop on Intersubband Transitions in Quantum Wells,* Cargese, France Sept. 9-14, 1991, edited by E. Rosencher, B. Vinter, and B. F. Levine (Plenum, London, 1992).

3) J. Y. Andersson and L. Lundqvist, Appl. Phys. Lett. S9, 857 (1991).

4) S. D. Gunapala, B. F. Levine, D. Ritter, R. A. Harem, and M. B. Panish, Appl. Phys. Lett. 58,2024 (1991).

5) S. D. Gunapala, B. F. Levine, D. Ritter, R. A. Harem, and M. B. Panish, Appl. Phys. Lett. 60,636 (1992).

6) B. K. Janousek, M. J. Daugherty, W. I.. Bloss, M. L. Rosen bluth, M. J. 0'1 .oughlin, H. Kanter, F. J. Dc Luccia, and L. E. Perry, J. Appl. Phys. 67,7608 (1990).

7) S. R. Andrews and B. A. Miller, J. Appl. Phys. 70,993 (1 991).

8) K. K. Choi, M. Dutta, P. G. Newman, M. L. Saunders, and G. L. Iafrate, Appl. Phys. Lett. S7, 1348 (1990).

9) L. S. Yu and S. S. Li, Appl. Phys. Lett. 59, 1332 (1991).

10) A. G. Steele, H. C. Liu, M. Buchanan, and Z. R. Wasilewski, Appl. Phys. Lett. S9, 3625 (1991).

11) S. D. Gunapala, B. F. Levine, L. Pfeiffer, and K. West, J. Appl. Phys. 69, 6517 (1990).

12) M. J. Kane S. Millidge, M. T. Emeny, D. Lee, D. R. P. Guy, and C. R. Whitehouse in Ref. 2.

13) C. S. Wu, C. P. Wen, R. N. Sate, M. Hu, C. W. Tu, J. Zhang, 1.. D. Flesner, L. Pham, and P. S. Nayer, IEEE Tran. Electron Devices 39, 234 (1992).

14) K. K. Choi, M. Dutta, and R. P, Moerkirk, Appl. Phys. Lett. **58**, 1533 (1991).

15) K. K. Choi, M. Taysing-Lara, L. Fotiadis, and W. Chang, Appl. Phys. Lett. S9, 1614 (1991).

16) K. K. Choi, L. Fotiadis, M. Taysing-Lara, and W. Chang, Appl. Phys. Lett. 59, 3303 (1991).

17) B. F. Levine, C. G. Bethea, K. G. Glogovsky, J. W. Stayt, and R. E. Labenguth, Semicon. Sci. Technol. 6 (1991) cl 14.

18) M. T. Asom et al., Proceedings of the IRIS Specialty Group on Infrared Materials, Boulder, CO, August 12-16,1991, Vol. **1**, p. 13.

19) L. J. Kozlowski, G. M. Williams, G. J. Sullivan, C. W. Farley, R. J. Anderson, J. K. Chen, D. T. Cheung, W. E. Tennant, and R. F. DeWames, IEEE Trans. Electron Devices 38, 1124 (1991).

20) B. F. Levine, C. G. Bethea, G. Hasnain, V. O. Shen, E. Pelve, R. R. Abbott, and S. J. Hsieh, Appl. Phys. Lett. S6, 851 (1990).

21) B. F. Levine, R. J. Malik, J, Walker, K. K. Choi, C. G. Bethea, D. A. Kleinman, and J. M. Vandenberg, Appl. Phys. Lett. 50,2.73 (1987).

22) G. Hasnain, B. F. Levine, C. G. Bethea, R. R. Abbott, and, S. J. Hsieh, J. Appl. Phys. 67,4361 (1990).

23) M. O. Manasreh, F. Szmuiowicz, D. W. Fischer, K. R. Evans, and C. E. Stutz, Appl. Phys. Lett. 57, 1790 (1990).

24) B. F. Levine, A. Zussman, S. D. Gunapala, M. T. Asom, J. M. Kuo, and W. S. Hobson, J. Appl. Phys. 72,4429 (1992).

FIGURE CAPTIONS

Fig.1 Theoretical and experimental (solid) dark current-voltage curves at T = 60K. Dotted curve shows the dark current (theoretical) due to thermionic emission only. Dashed curve shows the total dark current (thermionic + tunneling + thermionic assisted) versus bias voltage.

Fig.2 Conduction-band diagram of a infrared hot electron transistor, which utilizes bound to continuum intersubband transition,

Fig.3 Absorption coefficient spectra $\alpha(\lambda)$ of the *long* wavelength quantum well infrared detector. This absorption spectra was measured at room temperature using a 45° multipass waveguide geometry as shown in the inset.

Fig.4 IHET emitter and collector dark currents versus base-collector voltage at T = 60K. Emitter bias was kept at -1 V relative to the base potential. This figure also shows the lower energy dark current filtration capability of the quantum filter.

Fig.5 The emitter (QWIP) and collector (IHET) responsivity spectrums at T = 60K. Emitter was kept at -1 V bias relative to the base and collector.

Fig.6 IHET emitter and collector photo currents Vs base-collector voltage at T = 60K. Emitter was kept at -1 V bias relative to the base potential.

FIG. 7 Peak defectivity D* for a IHET having a cut-off wavelength of = 17.3 μm as a function of temperature T.

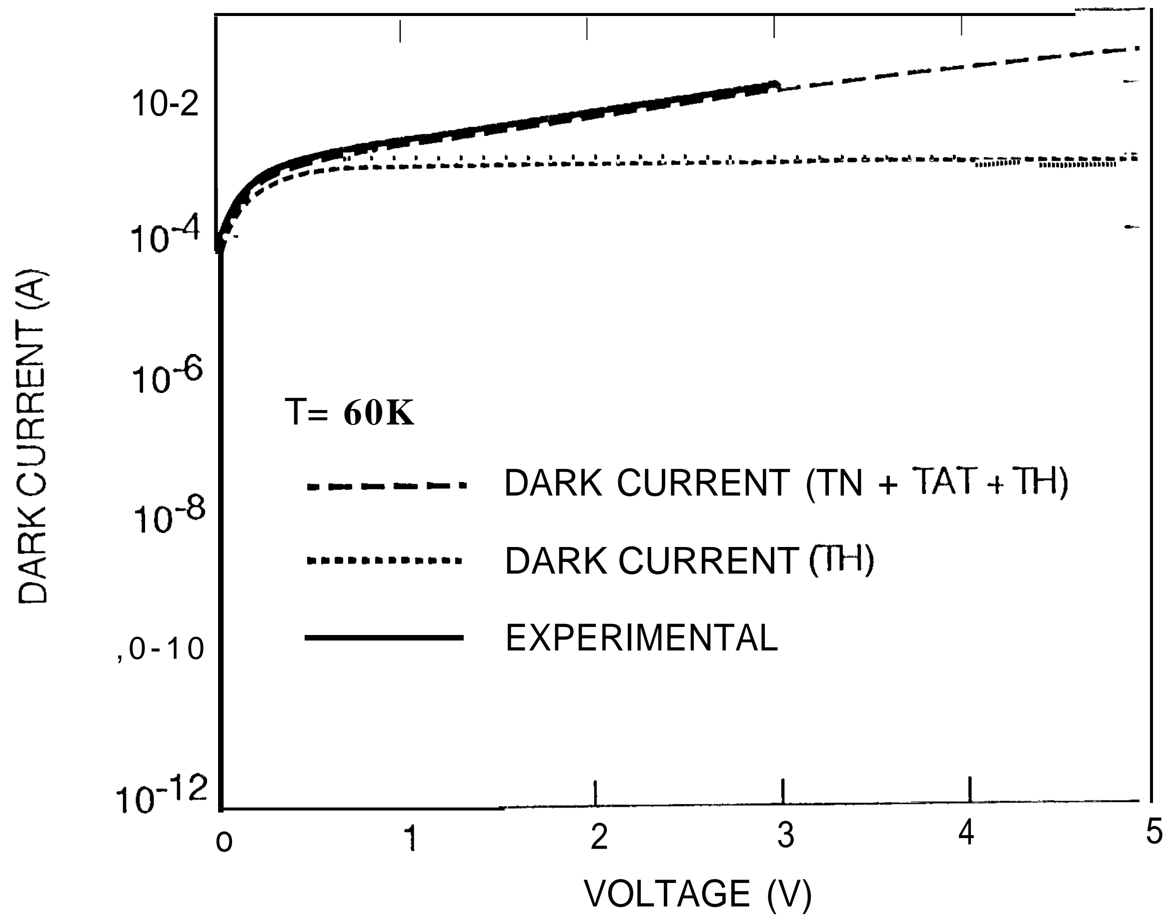
10-2
10-4
10-6
10-8
,0-10
10-12
DARK CURRENT (A)
T= 60K
DARK CURRENT (TN + TAT + TH)
DARK CURRENT (TH)
EXPERIMENTAL
0
1
2
3
4
5
VOLTAGE (V)

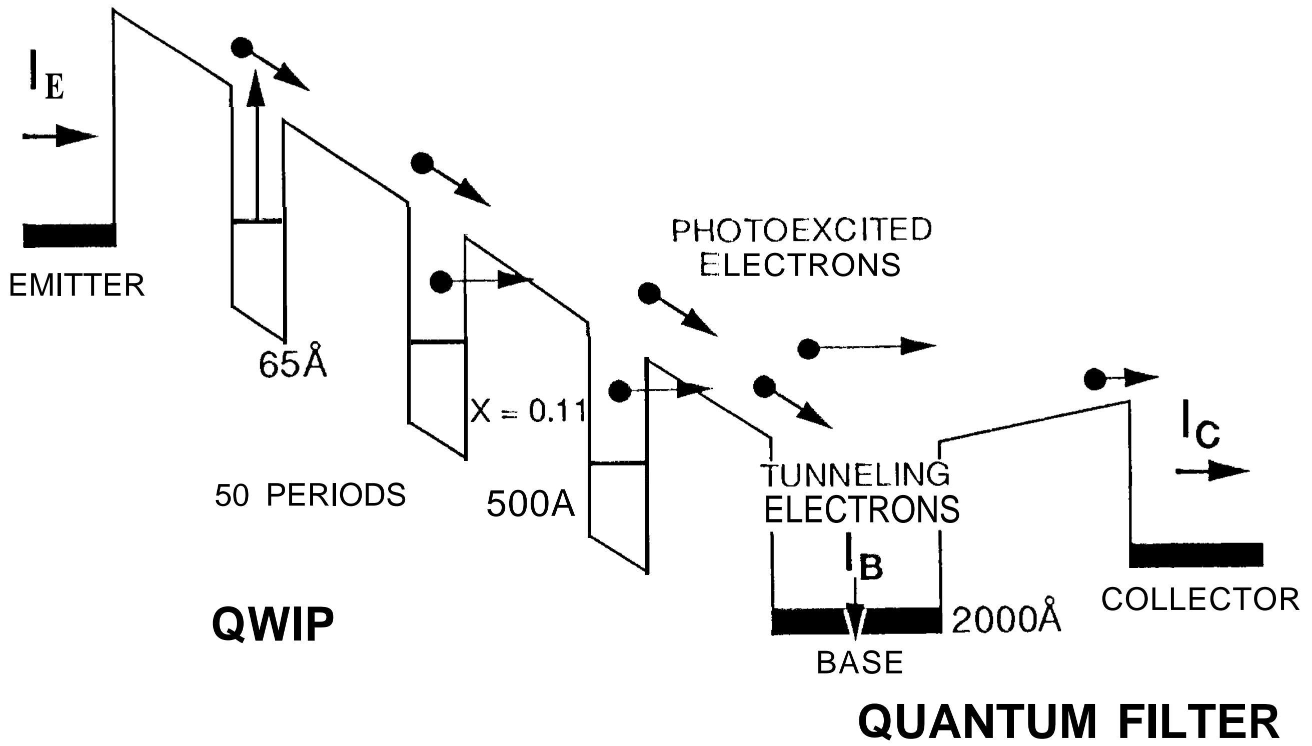

I_E
EMITTER
65Å
50 PERIODS
X = 0.11
500A
PHOTOEXCITED ELECTRONS
TUNNELING ELECTRONS
I_B
BASE
2000Å
I_C
COLLECTOR
QWIP
QUANTUM FILTER

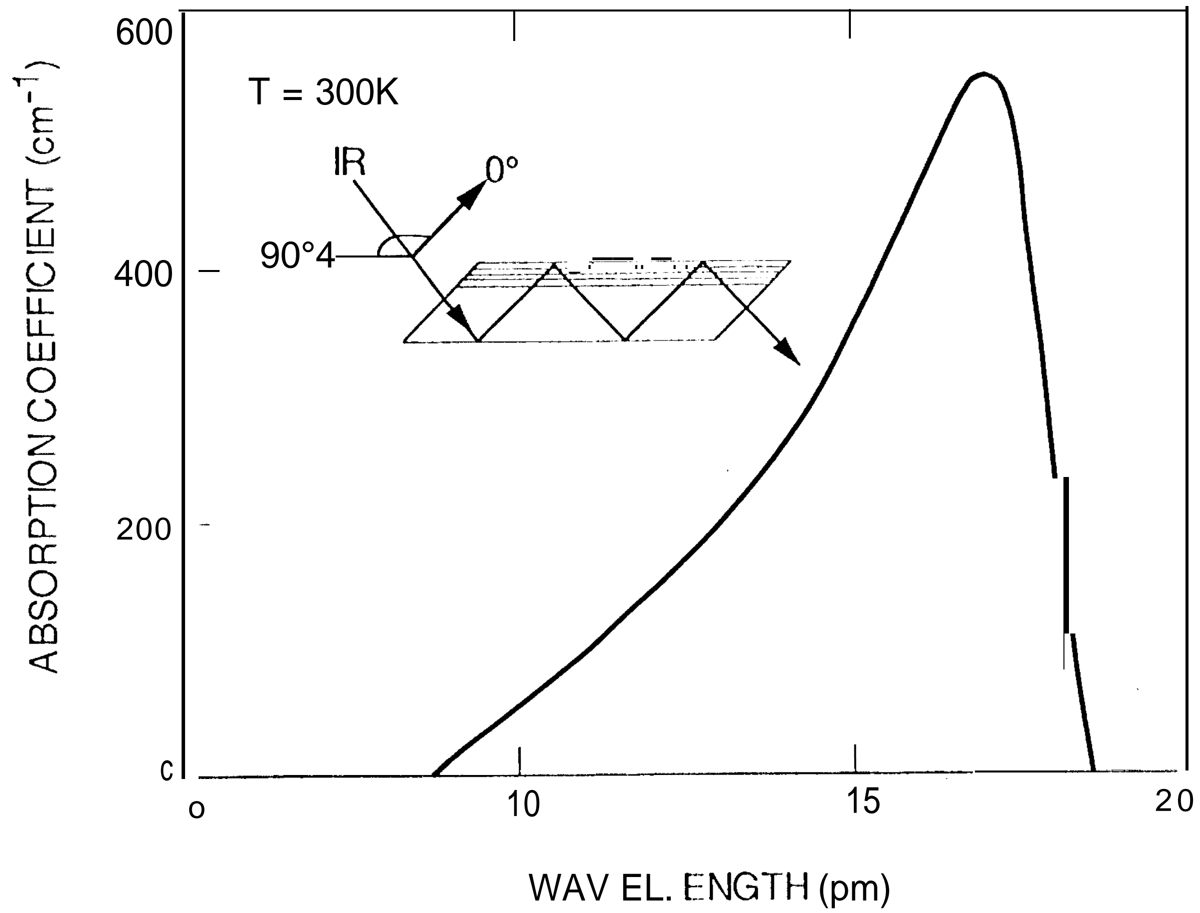

ABSORPTION COEFFICIENT (cm^{-1})
600
400
200
c
T = 300K
IR
0°
90°4
o
10
15
20
WAV EL. ENGTH (pm)

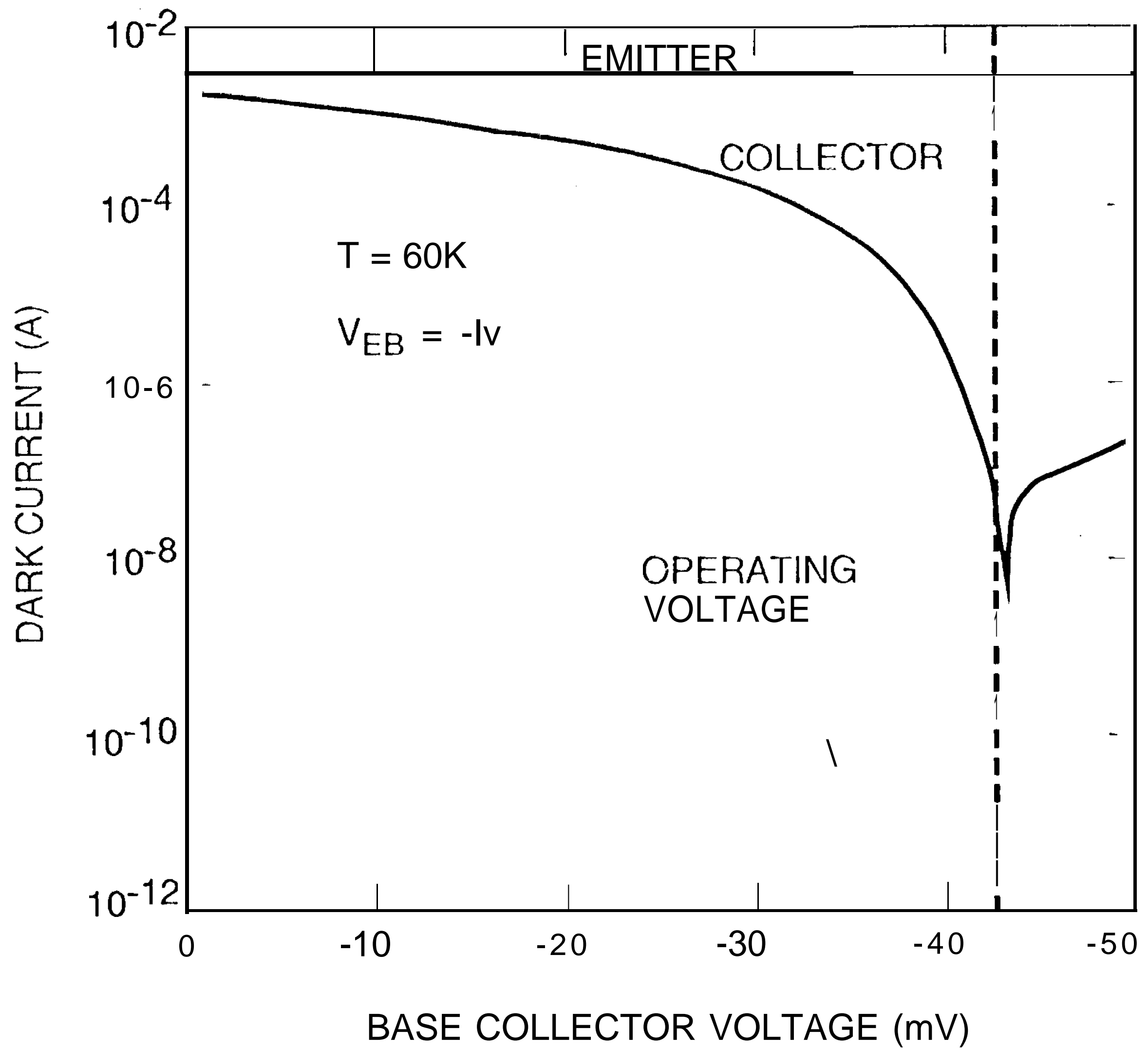
EMITTER
COLLECTOR
T = 60K
V_EB = -Iv
OPERATING
VOLTAGE
DARK CURRENT (A)
10-2
10-4
10-6
10-8
10-10
10-12
0
-10
-20
-30
-40
-50
BASE COLLECTOR VOLTAGE (mV)

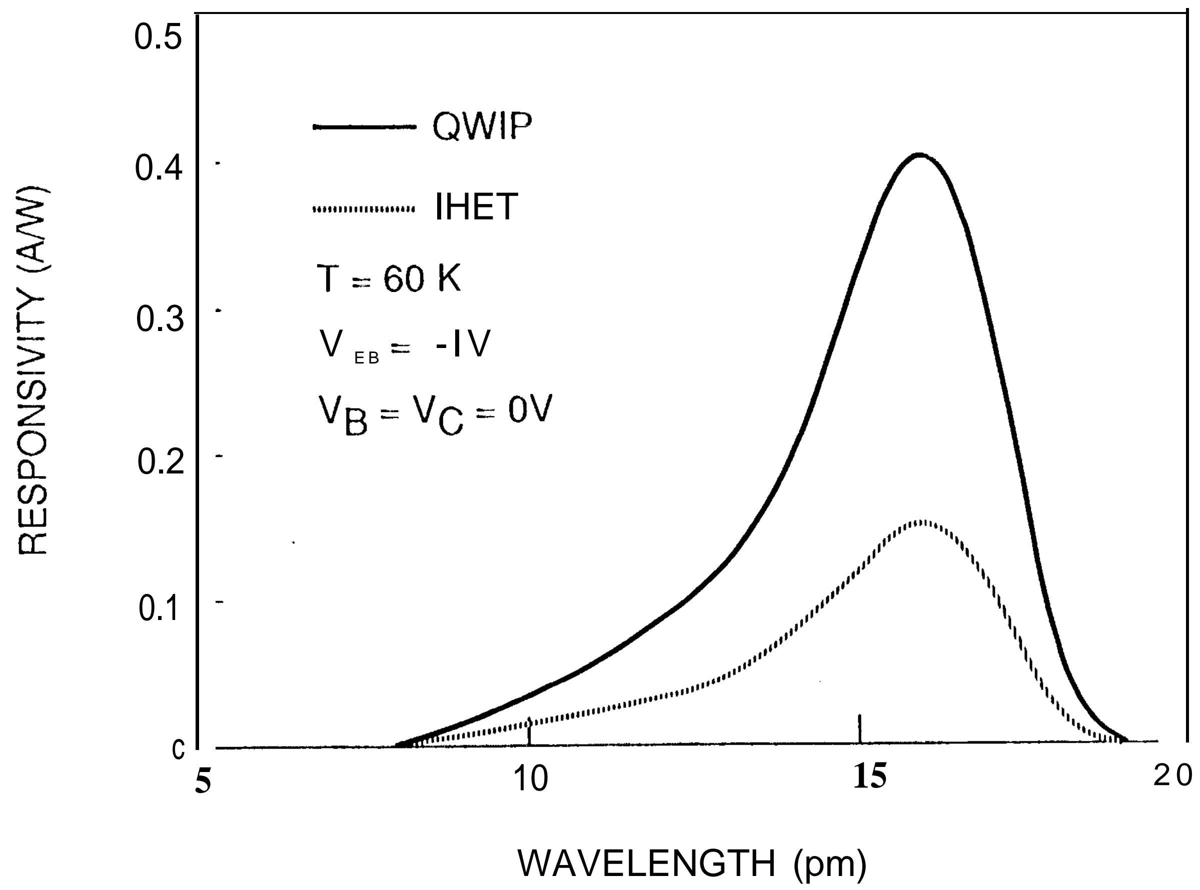
0.5
0.4
0.3
0.2
0.1
C
QWIP
IHET
T = 60 K
V EB = -IV
VB = VC = 0V
RESPONSIVITY (A/W)
5
10
15
20
WAVELENGTH (pm)

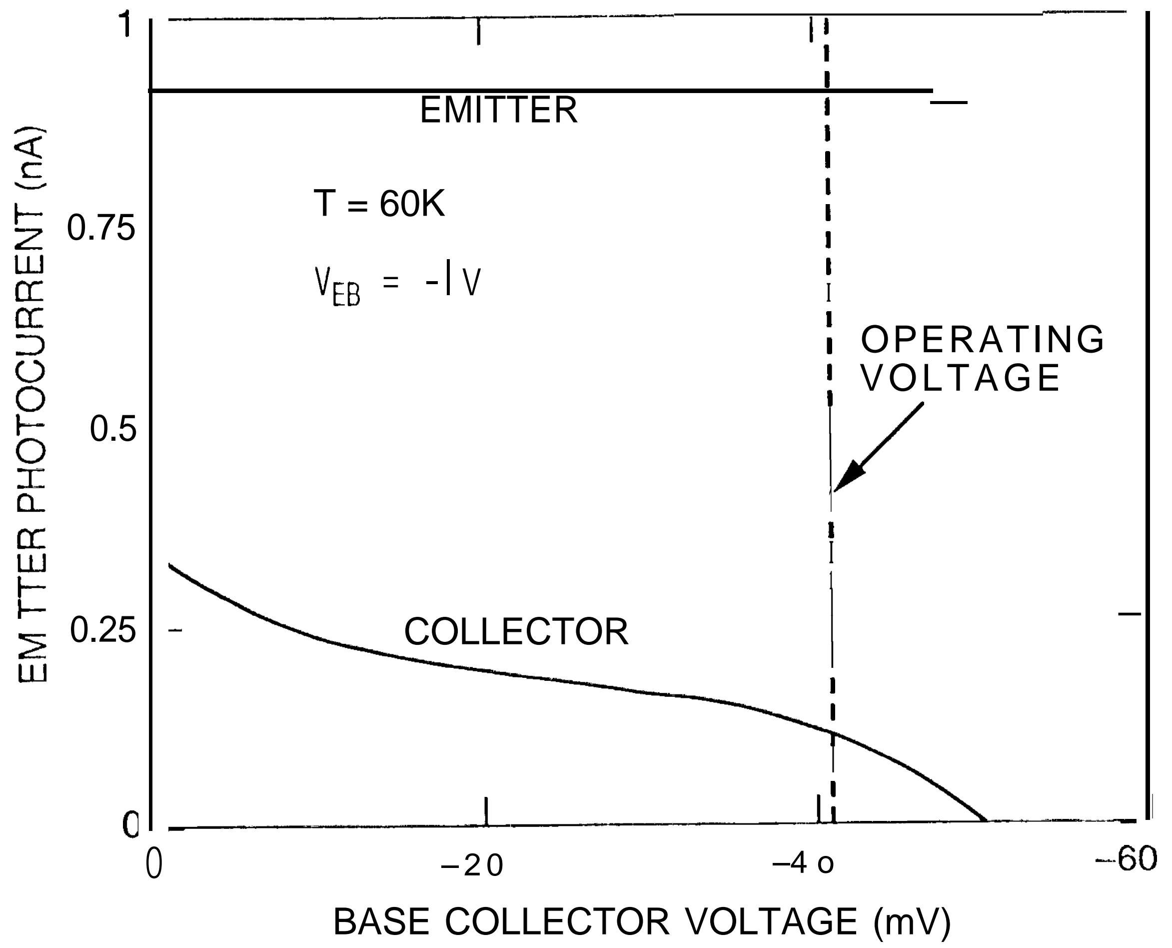
EMITTER
T = 60K
V_{EB} = -1V
OPERATING
VOLTAGE
COLLECTOR
EM TTER PHOTOCURRENT (nA)
1
0.75
0.5
0.25
0
0
−20
−4 o
−60
BASE COLLECTOR VOLTAGE (mV)

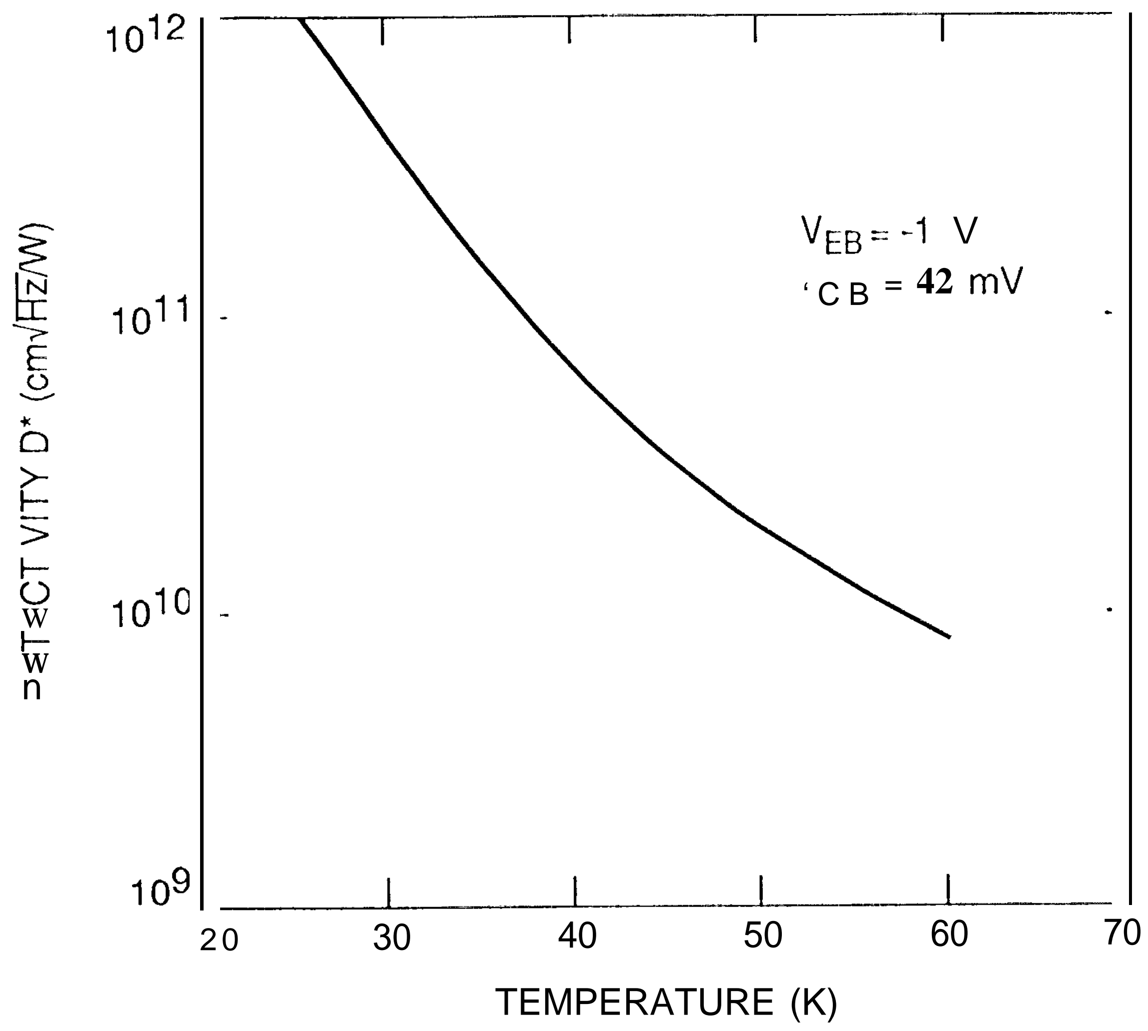

10^{12}
10^{11}
10^{10}
10^{9}
VITY D* (cm√Hz/W)
V_{EB} = -1 V
'C B = 42 mV
20
30
40
50
60
70
TEMPERATURE (K)